

# MSA<sup>2</sup>Net: Multi-scale Adaptive Attention-guided Network for Medical Image Segmentation

Sina Ghorbani Kolahi<sup>1</sup>  
sina.ghorbani@modares.ac.ir

Seyed Kamal Chaharsooghi<sup>1</sup>  
skch@modares.ac.ir

Toktam Khatibi<sup>1</sup>  
toktam.khatibi@modares.ac.ir

Afshin Bozorgpour<sup>2</sup>  
afshin.bozorgpour@ur.de

Reza Azad<sup>2,3</sup>  
reza.azad@rwth-aachen.de

Moein Heidari<sup>4</sup>  
moein.heidari@ubc.ca

Ilker Hacihaliloglu<sup>4</sup>  
ilker.hacihaliloglu@ubc.ca

Dorit Merhof<sup>2,5</sup>  
dorit.merhof@ur.de

<sup>1</sup> Tarbiat Modares University  
Tehran, Iran

<sup>2</sup> University of Regensburg  
Regensburg, Germany

<sup>3</sup> RWTH Aachen University  
Aachen, Germany

<sup>4</sup> University of British Columbia  
British Columbia, Canada

<sup>5</sup> Fraunhofer Institute for Digital Medicine  
MEVIS  
Bremen, Germany

## Abstract

Medical image segmentation involves identifying and separating object instances in a medical image to delineate various tissues and structures, a task complicated by the significant variations in size, shape, and density of these features. Convolutional neural networks (CNNs) have traditionally been used for this task but have limitations in capturing long-range dependencies. Transformers, equipped with self-attention mechanisms, aim to address this problem. However, in medical image segmentation it is beneficial to merge both local and global features to effectively integrate feature maps across various scales, capturing both detailed features and broader semantic elements for dealing with variations in structures. In this paper, we introduce MSA<sup>2</sup>Net, a new deep segmentation framework featuring an expedient design of skip-connections. These connections facilitate feature fusion by dynamically weighting and combining coarse-grained encoder features with fine-grained decoder feature maps. Specifically, we propose a Multi-Scale Adaptive Spatial Attention Gate (MASAG), which dynamically adjusts the receptive field (Local and Global contextual information) to ensure that spatially relevant features are selectively highlighted while minimizing background distractions. Extensive evaluations involving dermatology, and radiological datasets demonstrate that our MSA<sup>2</sup>Net outperforms state-of-the-art (SOTA) works or matches their performance. The source code is publicly available at <https://github.com/xmindflow/MSA-2Net>.

# 1 Introduction

Medical image segmentation is a crucial for disease diagnosis and quantitative assessment across the entire clinical workflow [1]. This technology is especially critical in biomedical applications, where detecting individual tumors, organs, or cell entities and segmenting their shapes represents a major bottleneck [2]. The inherent challenges of automated segmentation arise from the considerable variations in the size, shape, appearance, and density of the object of interest. Deep learning networks excel in medical image analysis, outperforming traditional SOTA techniques. The fully convolutional neural network (FCN) stands out as one of the pioneering approaches employed for image segmentation [3]. The seminal U-Net [4], featuring a series of convolutional and down-sampling layers to gather contextual information along its contracting path, with skip connections from the encoder to up-sample both coarse and fine features, has demonstrated eminent segmentation potential. The CNN and U-Net architectures have been enhanced through various adaptations aimed at optimizing their performance. Innovations have included the introduction of attention mechanisms [5], the incorporation of dynamic modeling [6, 7, 8], modifying skip connections [9], and the replacement of backbone modules within segmentation networks [10]. These enhancements have been critical in advancing the capabilities of these architectures to handle the complexities of medical image segmentation. While CNNs have traditionally been preferred for this task, they struggle to effectively model long-range dependencies and are limited by static receptive fields, which restrict their ability to capture the shape and structural details needed for precise medical image segmentation. The Vision Transformer (ViT) [11] was designed to address this limitation. Equipped with the self-attention mechanism, ViTs excel at capturing global information and modeling long-range dependencies. However, transformers are limited in capturing the local representation and context and are computationally inefficient with quadratic complexity. Several methods have been proposed to overcome the disadvantages of the transformer model [12], such as hybrid CNN-Transformer architectures [13, 14], reducing the computational cost of self-attention [15], performing the self-attention mechanism in local regions [16], or calculating channel attention instead of spatial attention [17]. However, these methods capture only partially the global context while addressing the diverse challenges in medical images, such as variations in form, visual characteristics, and compactness, necessitating the integration of both local and global features. A feasible approach in addressing the inherent limitations of the aforementioned architectures with respect to local and global information processing is the use of skip connections [18]. In medical image segmentation, capturing both local details (like the texture of tissues) and global context (such as the structure of organs) is crucial. Skip connections help in preserving high-resolution details through the network layers, enabling the model to use both fine and coarse features for more precise segmentation. Skip connections assist CNNs by reintegrating precise local features from initial layers into deeper ones, blending detailed and broad information for comprehensive contextual understanding [19], thus overcoming their naturally limited receptive fields. For transformers, skip connections enhance performance by integrating local details directly into layers focused on global processing, effectively balancing local precision with global awareness. However, most of these studies have focused solely on improving the encoder or decoder, and not on altering the original skip connection design as such [20]. Therefore, we propose MSA<sup>2</sup>Net, augmented by innovative skip connections that incorporate our novel Multi-Scale Adaptive Spatial Attention Gate (MASAG). This module strategically highlights spatially relevant features across multiple scales, enabling it to effectively model complex structures for delineating and localizing

objects of interest. This stage facilitates a spatial interplay between local and global features, enriching the feature maps with a nuanced, contextually informed representation [14]. Within the decoder, initial layers employ the Large Kernel Attention (LKA) module [16] for adept local and global feature management, addressing typical high-resolution image processing challenges in transformers. Deeper layers of the decoder use Dual Attention Enhanced Transformer blocks (DAE-Former) [6], effectively preserving long-range interactions in lower-resolution images while incorporating both spatial and channel attentions seamlessly, thus maintaining the grid integrity of the images. This strategy guarantees accurate and context-sensitive delineation of anatomical features within intricate medical images.

**Contributions:** The key contributions of this paper are as follows: (i) The introduction of MASAG, which dynamically recalibrate the receptive fields to emphasize spatially relevant features and suppress irrelevant background details. (ii) A hybrid decoder that integrates DAE-Former blocks in deeper layers for low-resolution image processing and LKA modules in shallow layers for high-resolution detail management for accurate and boundary-aware segmentation. (iii) Extensive evaluation across two challenging medical datasets, namely dermatology (ISIC2018 [11]), and radiology (Synapse [9]) datasets, demonstrates that our method surpasses SOTA approaches across diverse metrics.

## 2 Related Work

**CNN-based Segmentation Networks:** Motivated by the remarkable success of the U-Net model [5], it has been widely adopted for various medical image segmentation tasks through backbone, bottleneck or skip connection enhancements [9, 18]. Oktay et al. [9] introduced a novel attention gate (AG) module to emphasize key features relevant to a specific task. Shen et al. [5] added a dynamic selective attention module based on selective convolution kernel [25] for learning the dependencies between the channels. However, in our method, channel attention has been altered to spatial attention to suppress irrelevant areas and highlight salient regions based on dynamic receptive fields to learn local and global contextual information.

**Transformer-based and Hybrid Segmentation Networks:** Transformers have demonstrated their capability to gather global information, addressing the drawback of CNNs in capturing long-range semantic dependencies and limited receptive fields. Some of these studies aim to capture long-range spatial context using purely transformer-based approaches instead of CNN-based methods, which partially broaden the receptive field of CNNs [39]. However, the quadratic computational complexity of transformers, along with their inefficiency in capturing local contextual relationships between intra-path pixels, limits their usability in dense vision tasks such as medical image segmentation, which requires the neighboring pixel dependencies to be considered in the multi-scale and hierarchical pattern [22]. To concurrently exploit the multi-scale representation along with the ability to capture local semantic and texture information of CNNs, and long-range interaction of transformers, cohort studies are dedicated to hybrid CNN-transformer based methods [6, 10, 32]. Specifically, Swin-UNet [8] and DS-TransUNet [26] introduce models with a U-shaped structure that utilizes the Swin Transformer [27] for 2D image segmentation.

**Improving Skip-connections in Segmentation Networks:** Methods for redesigning skip-connections broadly attempt to process the encoder feature maps passed through the skip connections [43], combine the two sets of feature maps [29], or extend the number of skip-connections [24]. Despite these efforts, previous methods often encounter limitations with

fixed receptive fields and simplistic fusion methods in skip connections, such as addition or concatenation [29, 80, 60], which overlook content variance present in medical images. To address this, we incorporate MASAG into our hybrid CNN-Transformer, which provides a multi-scale strategy and enhanced feature fusion. MASAG dynamically tunes spatial receptive fields and applies selective spatial weights, sharpening the focus on essential features while minimizing background noise and reducing false positives. This approach not only enriches the feature maps with local-global contextual information, crucial for accurate segmentation of varied organ shapes and sizes, but also recalibrates the encoder’s output with a detailed spatial attention map.

## 3 Methodology

### 3.1 Motivation

Our methodology, motivated by the complexity of medical image segmentation and the limitations of previous architectures, employs a context-sensitive framework with adaptive skip connections to better capture anatomical details. This adaptive framework is pivotal in merging the encoder’s high spatial resolution with the decoder’s semantically rich features for optimized feature fusion. Essential to this process is a module within the skip connections that dynamically accentuates vital features and selectively focuses on relevant regions, harmonizing local details with a broader contextual understanding. This strategy is critical to minimizing background noise and highlighting key areas, underpinned by a boundary-aware approach in both the proposed module and the loss function. Furthermore, the deliberate configuration of decoder networks is key, ensuring the cohesive fusion of detailed and semantic features, while addressing the local and global feature processing gaps inherent in transformer and convolutional models.

### 3.2 Overall Architecture

The overall architecture of our novel method, named MSA<sup>2</sup>Net, as illustrated in Figure 1. The proposed method leverages the MaxViT [58] hierarchical transformer in the encoder to effectively capture multi-scale features through a combination of MBConv [63] and various attention mechanisms. Enhanced by innovative skip connections that include our novel MASAG module, the method ensures that spatially relevant features are selectively emphasized while background distractions are minimized due to dynamically adjust of the spatial receptive fields, guided by inputs from both the encoder and decoder. Moreover, MASAG introduces a spatial interaction stage, enabling a bidirectional process between local and global features, thus providing the feature maps with a detailed, contextually informed representation. The decoder’s shallow layers employ the LKA [16] modules to adeptly balance local and global features as well as channel interactions, overcoming typical high-resolution image processing challenges associated with self-attention. Deeper decoder layers utilize DAE-Former blocks [6] to efficiently maintain long-range dependencies in lower-resolution images, integrating spatial and channel attentions without disrupting the 2D structure of images. Overall, this method aims at accurate, context-aware segmentation of anatomical structures in complex medical images.

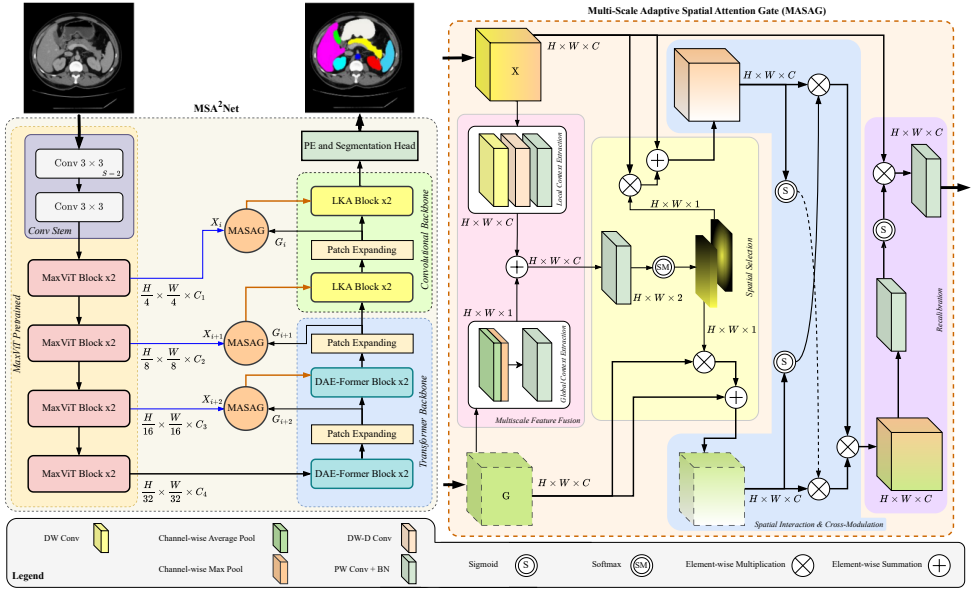


Figure 1: Our proposed segmentation network, called  $MSA^2Net$ , is composed of an encoder (using pretrained *MaxViT* block) and a decoder (comprising DAE-Former blocks in deeper layers and LKA blocks in shallow ones). The encoding-decoding feature fusion is performed via our novel MASAG module.

### 3.3 Multi-Scale Adaptive Spatial Attention Gate (MASAG)

Addressing the variability in organ structures, sizes, and shapes is a significant challenge. Traditional methods often rely on fixed receptive fields and simplistic fusion techniques in skip connections, failing to capture content diversity. To address this, we introduce the MASAG within our hybrid CNN-Transformer architecture’s skip connections to enhance segmentation accuracy. MASAG, with its four stages – *multi-scale fusion*, *spatial selection*, *spatial interaction and cross-modulation*, and *recalibration* – processes encoder and decoder outputs ( $\mathbf{X}$  and  $\mathbf{G}$ , respectively). The multi-scale fusion is utilized to aggregate  $\mathbf{X}$  and  $\mathbf{G}$  in a semantically similar way, preparing the fused feature map for subsequent processing. Spatial selection dynamically adjusts receptive fields to prioritize essential features, while spatial interaction and cross-modulation enrich feature maps with both local details and global context. In the recalibration stage, the initial input from encoder is refined using a dynamically generated, selective attention map from MASAG, ensuring spatial precision in segmentation. This approach allows MASAG to effectively navigate the diverse challenges of medical imaging, guaranteeing precise and dependable segmentation outcomes. Each stage of MASAG will be explained in detail, elucidating the structured approach and operational workflow, as highlighted in Figure 1 (right side).

#### 3.3.1 Multi-Scale Feature Fusion

The MASAG module’s multi-scale feature fusion level integrates *Local Context Extraction* and *Global Context Extraction* to blend the encoder’s high-resolution spatial details ( $\mathbf{X}$ )

with the decoder’s semantic information ( $\mathbf{G}$ ). *Local Context Extraction* broadens the spatial scope of  $\mathbf{X}$  using depthwise and dilated convolutions, while *Global Context Extraction* captures wide-ranging contextual information from  $\mathbf{G}$  via channel-wise poolings. This integration forms a comprehensive feature map, crucial for the Spatial Selection stage in MASAG, ensuring accurate segmentation across diverse anatomical features. The multi-scale feature fusion is formulated as follows:

$$\mathbf{U} = \underbrace{\text{Conv}_{1 \times 1}(\text{DW-D}(\text{DW}(\mathbf{X})))}_{\text{Local Context Extraction}} + \overbrace{\text{Conv}_{1 \times 1}([\text{P}_{\text{Avg}}(\mathbf{G}); \text{P}_{\text{Max}}(\mathbf{G})])}^{\text{Global Context Extraction}}. \quad (1)$$

Here, DW and DW-D denote depthwise and dilated convolutions, and  $\text{Conv}_{1 \times 1}$  is point-wise convolution for *Local Context Extraction*, while  $\text{P}_{\text{Max}}$  and  $\text{P}_{\text{Avg}}$  represent max and average pooling for *Global Context Extraction*, The notation  $[\cdot]$  signifies concatenation.

### 3.3.2 Spatial Selection

In the Spatial Selection stage of MASAG, the fused feature map ( $\mathbf{U}$ ), obtained from Equation 1 is projected to two channels, aligning with inputs  $\mathbf{X}$  and  $\mathbf{G}$ . Spatially selective weights, calculated via a channel-wise softmax, refine attention across  $\mathbf{X}$  and  $\mathbf{G}$ , leading to spatially selected versions  $\mathbf{X}'$  and  $\mathbf{G}'$ . These versions emphasize key areas while minimizing less relevant ones, enhancing receptive field selection. Additionally, two residual connections for  $\mathbf{X}'$  and  $\mathbf{G}'$  improve gradient flow and feature utilization, further refining the segmentation with precise, context-aware attention. The formulation of this process is as follows:

$$\begin{aligned} \text{SW}_i &= S(\text{Conv}_{1 \times 1}(\mathbf{U})) \quad \forall i \in [1, 2], \\ \mathbf{X}' &= \text{SW}_1 \otimes \mathbf{X} + \mathbf{X}, \quad \mathbf{G}' = \text{SW}_2 \otimes \mathbf{G} + \mathbf{G}, \end{aligned} \quad (2)$$

where  $\text{SW}_i \in \mathbb{R}^{2 \times H \times W}$ , derived via channel-wise softmax ( $S$ ), ensures that the weights across two channels ( $i \in [1, 2]$ ) sum to 1 at each spatial location, indicating the relative contribution of inputs according to content.

### 3.3.3 Spatial interaction and Cross-Modulation

The Spatial Interaction and Cross-Modulation level within MASAG *dynamically* enhances segmentation by weaving together the spatially refined inputs  $\mathbf{X}'$  and  $\mathbf{G}'$  (derived from Equation 3). Here,  $\mathbf{X}'$  with its refined local detail, is enriched by global contexts from  $\mathbf{G}'$ , through spatial weights applied via a *sigmoid*, creating  $\mathbf{X}''$ . Conversely,  $\mathbf{G}'$ , initially embodying weighted broader contexts, incorporates detailed contexts from  $\mathbf{X}'$ , evolving into  $\mathbf{G}''$ . This mutual enhancement ensures that both  $\mathbf{X}''$  and  $\mathbf{G}''$  integrate a comprehensive mix of local and global contexts, solidified by fusing  $\mathbf{X}''$  and  $\mathbf{G}''$  via multiplication, this integration combines detailed precision with overarching insights, effectively segmenting complex structural variations. The formulation of spatial interaction is described as follows:

$$\begin{aligned} \mathbf{X}'' &= \mathbf{X}' \otimes \sigma(\mathbf{G}'), \quad \mathbf{G}'' = \mathbf{G}' \otimes \sigma(\mathbf{X}'), \\ \mathbf{U}' &= \mathbf{X}'' \otimes \mathbf{G}'', \end{aligned} \quad (4)$$

where,  $\sigma(\mathbf{G}')$  and  $\sigma(\mathbf{X}')$  refer to local and global spatial weights respectively, and  $\mathbf{U}'$  denotes multiplied fused feature map.

### 3.3.4 Recalibration

In the Recalibration stage, the fused feature map from Spatial Interaction and Cross-Modulation (Equation 5) is refined through a point-wise convolution, followed by a *sigmoid* activation, to create a focused attention map. This map is used to recalibrate  $\mathbf{X}$ , the initial input from the encoder, by multiplying it with the attention map and further processing through another point-wise convolution layer, enhancing  $\mathbf{X}$  with an adaptive multi-scale receptive field tailored by previous stages. This ensures  $\mathbf{X}$  is aptly prepared with precise, context-aware features for integration into the decoder, facilitating accurate segmentation. The detailed formulation of this recalibration process is shown as follows:

$$\mathbf{X} = \text{Conv}_{1 \times 1} (\sigma (\text{Conv}_{1 \times 1} (\mathbf{U}')) \otimes \mathbf{X}). \quad (6)$$

## 4 Experiments

### 4.1 Datasets

To evaluate our method, we use the Synapse dataset [9] that encompasses a multi-organ segmentation across 30 cases with 3779 axial abdominal clinical CT images. We align our evaluation protocol with the guidelines provided by [10]. Further, we extend our evaluation to the skin lesion segmentation challenge, using the ISIC 2018 dataset [11], which includes 2594 dermoscopy images paired with their respective ground truth annotations. We adopt the data splitting and preprocessing procedures as outlined in [9].

### 4.2 Implementaion Details

Our Model, developed using the PyTorch library, operates on an NVIDIA RTX 3090 GPU and processes input images resized to 224 x 224 pixels. We used the pretrained MaxViT model for encoding. For the Synapse dataset, we configured a batch size of 20, an SGD solver with a base learning rate of 0.05, a momentum of 0.9, and a weight decay of 0.0001, training over 700 epochs. The ISIC dataset employed a batch size of 16 and was trained for 50 epochs using an Adam optimizer with an initial learning rate of 0.0001. Additionally, our model incorporates the Boundary Difference over Union (BDou) Loss [12] to enhance boundary-aware segmentation, dynamically adjusting penalties based on object size.

### 4.3 Quantitative Results

Tables 1 and 2 provide a comprehensive comparison of our proposed MSA<sup>2</sup>Net method with previous SOTA approaches. In the Synapse dataset (Table 1), MSA<sup>2</sup>Net shows superior performance over the 2D version of D-LKA by 0.48%. D-LKA is a hybrid model that employs deformable convolution in its LKA block to dynamically adjust the receptive field, effectively capturing organs in various shapes, sizes, and structures. Our method also surpasses DAE-Former, which relies on a fully transformer architecture akin to MISSFormer and Swin-Unet, by 2.21%. Additionally, MSA<sup>2</sup>Net outperforms Hiformer, a multi-scale CNN-Transformer model, by 4.36% in Dice Similarity Coefficient (DSC) and achieves a 1.41 reduction in Hausdorff Distance (HD95) compared to the same. Our method exhibits notable improvements in the segmentation of the spleen, aorta, liver, pancreas, and left kidney, with particularly significant enhancements in the pancreas and aorta segments, where

increases of 1.59% and 1.13% are observed over the second-best method, respectively. The quantitative results from the Synapse dataset illustrate that models utilizing dynamic receptive field recalibration yield better outcomes for both small and large organs, showcasing MSA<sup>2</sup>Net’s advantages over 2D D-LKA. For the ISIC dataset, as detailed in Table 2, our model not only achieves the highest scores across most metrics, but also surpasses other methods by at least 1.24% in DSC. This improvement can be attributed to the effectiveness of our multi-scale feature fusion modules in better capturing features of the boundary areas. These collective findings underscore the efficacy of dynamic receptive field adjustments in our MSA<sup>2</sup>Net approach, confirming its potential to set new benchmarks in the field of medical image segmentation.

Methods	Params (M)	FLOPs (G)	Spl.	RKid.	LKid.	Gal.	Liv.	Sto.	Aor.	Pan.	Average	
											DSC $\uparrow$	HD95 $\downarrow$
TransUNet [14]	96.07	88.91	85.08	77.02	81.87	63.16	94.08	75.62	87.23	55.86	77.49	31.69
Swin-UNet [8]	27.17	6.16	90.66	79.61	83.28	66.53	94.29	76.60	85.47	56.58	79.13	21.55
MISSFormer [15]	42.46	9.89	91.92	82.00	85.21	68.65	94.41	80.81	86.99	65.67	81.96	18.20
ScaleFormer [16]	111.6	48.93	89.40	83.31	86.36	74.97	95.12	80.14	88.73	64.85	82.86	16.81
HiFormer-B [17]	25.51	8.045	90.99	79.77	85.23	65.23	94.61	81.08	86.21	59.52	80.39	14.70
DAEFormer [9]	48.07	27.89	91.82	82.39	87.66	71.65	95.08	80.77	87.84	63.93	82.63	16.39
PVT-CASCADE [18]	35.28	6.40	90.10	80.37	82.23	70.59	94.08	83.69	83.01	64.43	81.06	20.23
2D D-LKA Net [1]	101.64	19.92	91.22	84.92	88.38	73.79	94.88	84.94	88.34	67.71	84.27	20.04
<b>MSA<sup>2</sup>Net (Ours)</b>	112.77	15.56	92.69	84.24	88.30	74.35	95.59	84.03	89.47	69.30	84.75	13.29

Table 1: The evaluation outcomes of the suggested approach on the Synapse dataset are presented in this comparison. The highest performing result is highlighted in blue, while the second highest is indicated in red. The metrics include parameters, reported in millions (M), and FLOPS, quantified in billions (G). The DSC and HD95 values are provided for several abdominal organs: spleen (Spl), right kidney (RKid), left kidney (LKid), gallbladder (Gal), liver (Liv), stomach (Sto), aorta (Aor), and pancreas (Pan).

Methods	DSC	SE	SP	ACC
U-Net [19]	0.8545	0.8800	0.9697	0.9404
AttU-Net [20]	0.8566	0.8674	0.9863	0.9376
TransUNet [14]	0.8499	0.8578	0.9653	0.9452
FAT-Net [15]	0.8903	0.9100	0.9699	0.9578
Swin-UNet [8]	0.8946	0.9056	0.9798	0.9645
UCTransNet [21]	0.8838	0.8429	0.9825	0.9527
DermoSegDiff [9]	0.9005	0.8761	0.9811	0.9587
<b>MSA<sup>2</sup>Net (Ours)</b>	0.9129	0.8840	0.9557	0.9640

Table 2: Comparative analysis of the proposed method versus SOTA techniques on ISIC2018 benchmark. Blue indicates the best result, and red displays the second-best.

## 4.4 Qualitative Results

We showcase visual segmentation results for the Synapse (Figure 2) and ISIC (Figure 3) datasets to further demonstrate the capacity of our method. It is evident that the predictions closely match the actual anatomical structure of the organs in the Synapse dataset, maintaining detailed features at the edges and precisely identifying organ areas. Furthermore, a visual assessment of the ISIC dataset shows that the boundaries predicted by our proposed model closely align with the ground truth, surpassing earlier methods, particularly in complex cases characterized by intricate color distribution and irregular borders, owing to our boundary-aware model and the MASAG module, which ensures optimal feature fusion.

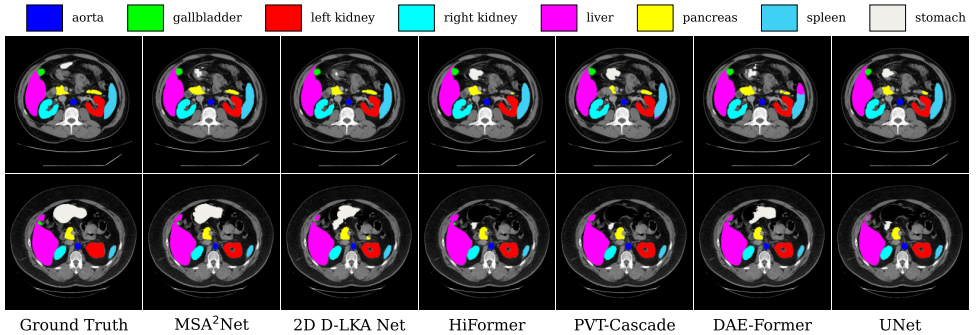


Figure 2: A comparative visual examination of the proposed approach in contrast to different methods employing the Synapse multi-organ segmentation dataset.

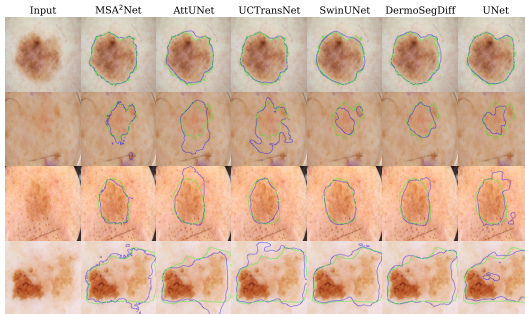


Figure 3: Visual comparisons of various techniques on the *ISIC2018* skin lesion segmentation dataset are depicted. Authentic boundaries are represented in green, while anticipated boundaries are depicted in blue.

## 4.5 Ablation Study

We conducted an ablation study on the Synapse dataset to examine the effectiveness of our modules under various configurations as summarized in Table 3. Specifically, the inclusion of MASAG (last three rows) demonstrates its capability to fine-tune focus adaptively, emphasizing key areas and dynamically adjusting features to enhance segmentation, as evidenced by improved DSC and reduced HD scores. Besides, the final row demonstrates that our design elements work together effectively, enhancing segmentation predictions by leveraging the synergistic effects of all components for superior detail preservation and precise organ delineation.

Model	MASAG	LKA	DAE-Former	Dice	HD95
MSA <sup>2</sup> Net	✗	✓	✗	82.80	17.42
MSA <sup>2</sup> Net	✗	✗	✓	83.16	16.18
MSA <sup>2</sup> Net	✗	✓	✓	83.76	14.42
MSA <sup>2</sup> Net	✓	✓	✗	84.32	15.14
MSA <sup>2</sup> Net	✓	✗	✓	84.41	14.82
MSA <sup>2</sup> Net	✓	✓	✓	<b>84.75</b>	<b>13.29</b>

Table 3: Ablation experiments on Synapse dataset: impact of individual contributions on segmentation performance of MSA<sup>2</sup>Net.

## 5 Conclusion

We proposed a novel medical image segmentation network to alleviate the restrictions of cohort studies in local and global information processing. Our key idea is to mitigate the limitations of fixed receptive sizes and basic fusion techniques in skip connections, thereby enhancing medical image segmentation, which is challenged by the variability in sizes and shapes of anatomical structures. We achieved this through a novel MASAG, which includes multi-scale fusion, spatial selection, interaction, cross-modulation, and recalibration. Our MSA<sup>2</sup>Net shows robust performance across two benchmark datasets compared to SOTA methods. Ablation studies confirm the effectiveness of the design and underlying assumptions of our approach.

## Acknowledgment

The authors gratefully acknowledge the computational and data resources provided by the Leibniz Supercomputing Centre ([www.lrz.de](http://www.lrz.de)).

## References

- [1] Alaaeldin Ali, Hugo Touvron, Mathilde Caron, Piotr Bojanowski, Matthijs Douze, Armand Joulin, Ivan Laptev, Natalia Neverova, Gabriel Synnaeve, Jakob Verbeek, et al. Xcit: Cross-covariance image transformers. *Advances in neural information processing systems*, 34:20014–20027, 2021.
- [2] Michela Antonelli, Annika Reinke, Spyridon Bakas, Keyvan Farahani, Annette Kopp-Schneider, Bennett A Landman, Geert Litjens, Bjoern Menze, Olaf Ronneberger, Ronald M Summers, et al. The medical segmentation decathlon. *Nature communications*, 13(1):4128, 2022.
- [3] Maryam Asadi-Aghbolaghi, Reza Azad, Mahmood Fathy, and Sergio Escalera. Multi-level context gating of embedded collective knowledge for medical image segmentation. *arXiv preprint arXiv:2003.05056*, 2020.
- [4] Reza Azad, Ehsan Khodapanah Aghdam, Amelie Rauland, Yiwei Jia, Atlas Haddadi Avval, Afshin Bozorgpour, Sanaz Karimijafarbigloo, Joseph Paul Cohen, Ehsan Adeli, and Dorit Merhof. Medical image segmentation review: The success of u-net. *arXiv preprint arXiv:2211.14830*, 2022.
- [5] Reza Azad, René Arimond, Ehsan Khodapanah Aghdam, Amirhossein Kazerouni, and Dorit Merhof. Dae-former: Dual attention-guided efficient transformer for medical image segmentation. In *International Workshop on PRedictive Intelligence In MEdicine*, pages 83–95. Springer, 2023.
- [6] Reza Azad, Leon Niggemeier, Michael Hüttemann, Amirhossein Kazerouni, Ehsan Khodapanah Aghdam, Yury Velichko, Ulas Bagci, and Dorit Merhof. Beyond self-attention: Deformable large kernel attention for medical image segmentation. In *Proceedings of the IEEE/CVF Winter Conference on Applications of Computer Vision*, pages 1287–1297, 2024.

- [7] Afshin Bozorgpour, Yousef Sadegheih, Amirhossein Kazerooni, Reza Azad, and Dorit Merhof. Dermosegdiff: A boundary-aware segmentation diffusion model for skin lesion delineation. In *International Workshop on PRedictive Intelligence In MEDicine*, pages 146–158. Springer, 2023.
- [8] Hu Cao, Yueyue Wang, Joy Chen, Dongsheng Jiang, Xiaopeng Zhang, Qi Tian, and Manning Wang. Swin-unet: Unet-like pure transformer for medical image segmentation. In *European conference on computer vision*, pages 205–218. Springer, 2022.
- [9] MICCAI 2015 Multi-Atlas Abdomen Labeling Challenge. Synapse multi-organ segmentation dataset. <https://www.synapse.org/#!/Synapse:syn3193805/wiki/217789>, 2015. Accessed: 2022-04-20.
- [10] Jieneng Chen, Yongyi Lu, Qihang Yu, Xiangde Luo, Ehsan Adeli, Yan Wang, Le Lu, Alan L Yuille, and Yuyin Zhou. Transunet: Transformers make strong encoders for medical image segmentation. *arXiv preprint arXiv:2102.04306*, 2021.
- [11] Noel Codella, Veronica Rotemberg, Philipp Tschandl, M. Emre Celebi, Stephen Dusza, David Gutman, Brian Helba, Aadi Kalloo, Konstantinos Liopyris, Michael Marchetti, Harald Kittler, and Allan Halpern. Skin lesion analysis toward melanoma detection 2018: A challenge hosted by the international skin imaging collaboration (isic), 2019.
- [12] Yimian Dai, Fabian Gieseke, Stefan Oehmcke, Yiquan Wu, and Kobus Barnard. Attentional feature fusion. In *Proceedings of the IEEE/CVF winter conference on applications of computer vision*, pages 3560–3569, 2021.
- [13] Alexey Dosovitskiy, Lucas Beyer, Alexander Kolesnikov, Dirk Weissenborn, Xiaohua Zhai, Thomas Unterthiner, Mostafa Dehghani, Matthias Minderer, Georg Heigold, Sylvain Gelly, et al. An image is worth 16x16 words: Transformers for image recognition at scale. *arXiv preprint arXiv:2010.11929*, 2020.
- [14] Qihang Fan, Huaibo Huang, Xiaoqiang Zhou, and Ran He. Lightweight vision transformer with bidirectional interaction. *Advances in Neural Information Processing Systems*, 36, 2024.
- [15] Mustansar Fiaz, Moein Heidari, Rao Muhammad Anwer, and Hisham Cholakkal. Sa2-net: Scale-aware attention network for microscopic image segmentation. 2022.
- [16] Meng-Hao Guo, Cheng-Ze Lu, Zheng-Ning Liu, Ming-Ming Cheng, and Shi-Min Hu. Visual attention network. *Computational Visual Media*, 9(4):733–752, 2023.
- [17] Moein Heidari, Amirhossein Kazerooni, Milad Soltany, Reza Azad, Ehsan Khodapanah Aghdam, Julien Cohen-Adad, and Dorit Merhof. Hiformer: Hierarchical multi-scale representations using transformers for medical image segmentation. In *Proceedings of the IEEE/CVF winter conference on applications of computer vision*, pages 6202–6212, 2023.
- [18] Huimin Huang, Lanfen Lin, Ruofeng Tong, Hongjie Hu, Qiaowei Zhang, Yutaro Iwamoto, Xianhua Han, Yen-Wei Chen, and Jian Wu. Unet 3+: A full-scale connected unet for medical image segmentation. In *ICASSP 2020-2020 IEEE international conference on acoustics, speech and signal processing (ICASSP)*, pages 1055–1059. IEEE, 2020.

- [19] Huimin Huang, Shiao Xie, Lanfen Lin, Yutaro Iwamoto, Xianhua Han, Yen-Wei Chen, and Ruofeng Tong. Scaleformer: revisiting the transformer-based backbones from a scale-wise perspective for medical image segmentation. *arXiv preprint arXiv:2207.14552*, 2022.
- [20] Xiaohong Huang, Zhifang Deng, Dandan Li, and Xueguang Yuan. Missformer: An effective medical image segmentation transformer. *arXiv preprint arXiv:2109.07162*, 2021.
- [21] Ali Karaali, Rozenn Dahyot, and Donal J Sexton. Dr-vnet: retinal vessel segmentation via dense residual unet. In *International Conference on Pattern Recognition and Artificial Intelligence*, pages 198–210. Springer, 2022.
- [22] Asifullah Khan, Zunaira Rauf, Abdul Rehman Khan, Saima Rathore, Saddam Hussain Khan, Najmus Saher Shah, Umair Farooq, Hifsa Asif, Aqsa Asif, Umme Zahoora, et al. A recent survey of vision transformers for medical image segmentation. *arXiv preprint arXiv:2312.00634*, 2023.
- [23] Salman Khan, Muzammal Naseer, Munawar Hayat, Syed Waqas Zamir, Fahad Shahbaz Khan, and Mubarak Shah. Transformers in vision: A survey. *ACM Computing Surveys*, 54(10s):1–41, January 2022. ISSN 1557-7341. doi: 10.1145/3505244. URL <http://dx.doi.org/10.1145/3505244>.
- [24] Haoming Li, Jinghui Fang, Shengfeng Liu, Xiaowen Liang, Xin Yang, Zixin Mai, Manh The Van, Tianfu Wang, Zhiyi Chen, and Dong Ni. Cr-unet: A composite network for ovary and follicle segmentation in ultrasound images. *IEEE journal of biomedical and health informatics*, 24(4):974–983, 2019.
- [25] Xiang Li, Wenhai Wang, Xiaolin Hu, and Jian Yang. Selective kernel networks. In *Proceedings of the IEEE/CVF conference on computer vision and pattern recognition*, pages 510–519, 2019.
- [26] Ailiang Lin, Bingzhi Chen, Jiayu Xu, Zheng Zhang, Guangming Lu, and David Zhang. Ds-transunet: Dual swin transformer u-net for medical image segmentation. *IEEE Transactions on Instrumentation and Measurement*, 71:1–15, 2022.
- [27] Ze Liu, Yutong Lin, Yue Cao, Han Hu, Yixuan Wei, Zheng Zhang, Stephen Lin, and Baining Guo. Swin transformer: Hierarchical vision transformer using shifted windows. In *Proceedings of the IEEE/CVF international conference on computer vision*, pages 10012–10022, 2021.
- [28] Jonathan Long, Evan Shelhamer, and Trevor Darrell. Fully convolutional networks for semantic segmentation. In *Proceedings of the IEEE conference on computer vision and pattern recognition*, pages 3431–3440, 2015.
- [29] Ozan Oktay, Jo Schlemper, Loic Le Folgoc, Matthew Lee, Mattias Heinrich, Kazunari Misawa, Kensaku Mori, Steven McDonagh, Nils Y Hammerla, Bernhard Kainz, et al. Attention u-net: Learning where to look for the pancreas. *arXiv preprint arXiv:1804.03999*, 2018.

- [30] Md Mostafijur Rahman and Radu Marculescu. Medical image segmentation via cascaded attention decoding. In *Proceedings of the IEEE/CVF Winter Conference on Applications of Computer Vision (WACV)*, pages 6222–6231, January 2023.
- [31] Olaf Ronneberger, Philipp Fischer, and Thomas Brox. U-net: Convolutional networks for biomedical image segmentation. In *Medical image computing and computer-assisted intervention—MICCAI 2015: 18th international conference, Munich, Germany, October 5-9, 2015, proceedings, part III 18*, pages 234–241. Springer, 2015.
- [32] Yousef Sadegheih, Afshin Bozorgpour, Pratibha Kumari, Reza Azad, and Dorit Merhof. Lhu-net: A light hybrid u-net for cost-efficient, high-performance volumetric medical image segmentation. *arXiv preprint arXiv:2404.05102*, 2024.
- [33] Mark Sandler, Andrew Howard, Menglong Zhu, Andrey Zhmoginov, and Liang-Chieh Chen. Mobilenetv2: Inverted residuals and linear bottlenecks. In *Proceedings of the IEEE conference on computer vision and pattern recognition*, pages 4510–4520, 2018.
- [34] Ramprasaath R Selvaraju, Michael Cogswell, Abhishek Das, Ramakrishna Vedantam, Devi Parikh, and Dhruv Batra. Grad-cam: Visual explanations from deep networks via gradient-based localization. In *Proceedings of the IEEE international conference on computer vision*, pages 618–626, 2017.
- [35] Longfeng Shen, Qiong Wang, Yingjie Zhang, Fenglan Qin, Hengjun Jin, and Wei Zhao. Dskca-unet: Dynamic selective kernel channel attention for medical image segmentation. *Medicine*, 102(39):e35328, 2023.
- [36] Zhuoran Shen, Mingyuan Zhang, Haiyu Zhao, Shuai Yi, and Hongsheng Li. Efficient attention: Attention with linear complexities. In *Proceedings of the IEEE/CVF winter conference on applications of computer vision*, pages 3531–3539, 2021.
- [37] Fan Sun, Zhiming Luo, and Shaozi Li. Boundary difference over union loss for medical image segmentation. In *International Conference on Medical Image Computing and Computer-Assisted Intervention*, pages 292–301. Springer, 2023.
- [38] Zhengzhong Tu, Hossein Talebi, Han Zhang, Feng Yang, Peyman Milanfar, Alan Bovik, and Yinxiao Li. Maxvit: Multi-axis vision transformer. In *European conference on computer vision*, pages 459–479. Springer, 2022.
- [39] Jeya Maria Jose Valanarasu, Poojan Oza, Ilker Hacihaliloglu, and Vishal M Patel. Medical transformer: Gated axial-attention for medical image segmentation. In *Medical Image Computing and Computer Assisted Intervention—MICCAI 2021: 24th International Conference, Strasbourg, France, September 27–October 1, 2021, Proceedings, Part I 24*, pages 36–46. Springer, 2021.
- [40] Haonan Wang, Peng Cao, Jiaqi Wang, and Osmar R Zaiane. Uctransnet: rethinking the skip connections in u-net from a channel-wise perspective with transformer. In *Proceedings of the AAAI conference on artificial intelligence*, volume 36, pages 2441–2449, 2022.
- [41] Peihao Wang, Wenqing Zheng, Tianlong Chen, and Zhangyang Wang. Anti-oversmoothing in deep vision transformers via the fourier domain analysis: From theory to practice. *arXiv preprint arXiv:2203.05962*, 2022.

- [42] Huisi Wu, Shihuai Chen, Guilian Chen, Wei Wang, Baiying Lei, and Zhenkun Wen. Fat-net: Feature adaptive transformers for automated skin lesion segmentation. *Medical Image Analysis*, 76:102327, 2022. ISSN 1361-8415. doi: <https://doi.org/10.1016/j.media.2021.102327>. URL <https://www.sciencedirect.com/science/article/pii/S1361841521003728>.
- [43] Tiange Xiang, Chaoyi Zhang, Dongnan Liu, Yang Song, Heng Huang, and Weidong Cai. Bio-net: learning recurrent bi-directional connections for encoder-decoder architecture. In *Medical Image Computing and Computer Assisted Intervention–MICCAI 2020: 23rd International Conference, Lima, Peru, October 4–8, 2020, Proceedings, Part I 23*, pages 74–84. Springer, 2020.

## Supplementary Material

In the supplementary material section, we provide comprehensive details about the MSA<sup>2</sup>Net parameters and offer insights into the frequency analysis of the proposed MASAG module. Moreover, we visualize the attention map of the output from our decoder layers using the GradCAM [24] technique to further demonstrate the effectiveness and contribution of the proposed modules. This is achieved by utilizing dynamic receptive field adjustment to capture long-range dependencies and local contextual relations among pixels, as demonstrated through GradCAM and spectral analysis.

### A Frequency Analysis of MSA<sup>2</sup>Net

Wang et al. [24] investigated a significant limitation of the self-attention mechanism. Through theoretical analysis, they demonstrated that self-attention functions as a low-pass filter, which removes high-frequency information and results in a loss of feature expressiveness in the model’s deep layers. The authors discovered that the Softmax operation causes self-attention to retain low-frequency information while losing fine details. In Figure A, we visualize the frequency response analysis of our method with the MASAG module compared to MSA<sup>2</sup>Net without it. It is evident that the standard design’s frequency response in the deep layers attenuates more than that with the presence of MASAG module. This visually demonstrates the model’s superior ability to preserve high-frequency details advantaging the MASAG module which can enhance high frequencies across all network layers and suppress irrelevant noise. Moreover, as shown in Figure A (bottom row, first column), the initial shallow layers of the decoder are prone to high-frequency details (owing to the fully transformer-based encoder), however, the incorporation of DAE-Former, LKA block, and the MASAG module aim in preserving high-frequency details, potentially affective in medical image segmentation. It should also be noted that high-frequency information is highly effective for capturing fine-grained details, especially when dealing with lesions and abnormalities that manifest as textures rather than shapes. Therefore, our MASAG module aids the network in preserving high-frequency information, which is crucial for detecting these irregular patterns.

### B Analysis of Parameters

In this section, we examine the exact number of parameters in various modules of MSA<sup>2</sup>Net. Our model consists of the MaxViT-B pretrained network utilized in the encoder section, while the skip connection section incorporates three MASAG modules, and the decoder structure comprises two DAE-Former modules in the lower layers and two LKA modules in the upper layers. Accordingly, the encoder section (MaxViT-B) has the highest number of parameters (Table A). Following this, the DAE-Former section, which is entirely transformer-based, has the second-highest number of parameters. The LKA module, which employs depth-wise convolution, has fewer parameters. Finally, the total number of parameters for the three MASAG modules is 9.44 million, making it an efficient structure in terms of parameter count. Notably, our main novel module, MASAG, is highlighted as a lightweight component, contributing only 8% of the parameters. Owing to its low parameter count, MASAG can play a crucial role as a plug-and-play module designed to enhance the performance of skip connections in various networks. This efficiency makes it an attractive option for integrating into other architectures to boost overall performance.

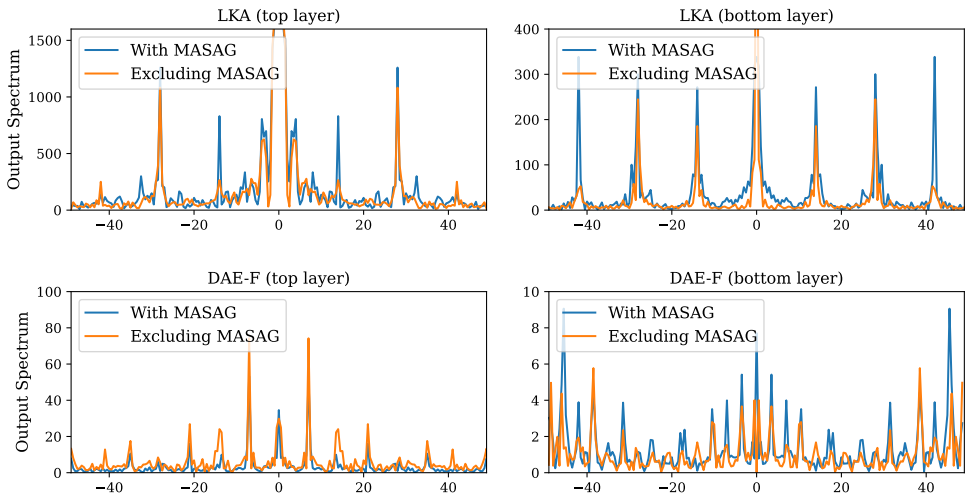


Figure A: Frequency response analysis on the  $MSA^2Net$  (with MASAG module present) vs.  $MSA^2Net$  (excluding MASAG module).

Structure	Module	Parameters (M)
Encoder	MaxViT-B	64.12
Skip Connection	MASAG	9.44
Decoder	LKA	1.37
	DAE-Former	37.84
Total		112.77

Table A: Details about the number of parameters in our model

## C Receptive Fields Analysis via GradCAM

The performance of the  $MSA^2Net$  model in detecting organs within the Synapse dataset was assessed by visualizing its attention map with GradCAM (Figure B). The results indicate that the  $MSA^2Net$  model is proficient at identifying small organs like the gallbladder and aorta, highlighting its ability to learn local features. Moreover, the model successfully detects larger organs, such as the liver and stomach, showcasing its capacity to capture long-range dependencies. In fact, the hybrid strategy employed in our model, incorporating the MASAG module, enables the simultaneous capture of both local and global patterns which stems from its ability in dynamic receptive field adjustment. This efficient approach significantly enhances segmentation performance by preserving high-frequency information essential for detecting fine-grained details and irregular textures, while also maintaining the ability to understand broader spatial relationships. This comprehensive capability ensures more accurate and reliable segmentation results across various organ types.

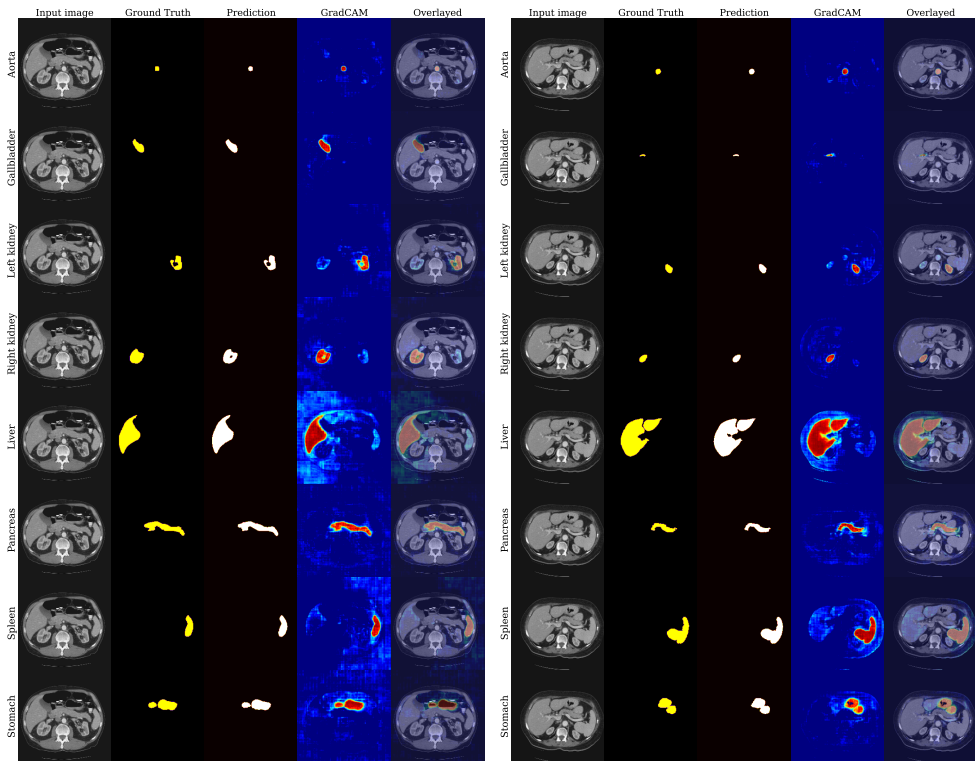


Figure B: Feature visualization comprising two samples from the last layer of our model with different organs of the Synapse dataset (first 4 rows with smaller organs and the other larger ones). The results exhibit that with the help of the MASAG module, MSA<sup>2</sup>Net is robust to the shape, size, and density variations of organs learned at the decoder.